Predictions of complete fusion cross sections of ^{6,7}Li, ^{9}Be, and ^{10}B with Bayesian neural network method*

Kaixuan Cheng,[1,†] Rongxing He,[1] Chunyuan Qiao,[1] and Chunwang Ma[1,2,‡]

[1]*School of Physics, Centre for Theoretical Physics, Henan Normal University, Xinxiang 453007, China*
[2]*Institute of Nuclear Science and Technology, Henan Academy of Sciences, Zhengzhou, 450015, China*

A machine learning approach utilizing the Bayesian neural networks has been developed to predict the complete fusion cross sections of weakly bound nuclei. This method was trained and validated using 475 experimental data points from 39 reaction systems all induced by ^{6,7}Li, ^{9}Be and ^{10}B. The constructed Bayesian neural network demonstrated a high degree of accuracy in evaluating the complete fusion cross sections. By comparing the predicted cross sections with those obtained from the single barrier penetration model, the suppression effect of ^{6,7}Li and ^{9}Be with stable nucleus was made a systematic analysis. In the cases of ^{6}Li and ^{7}Li, a less suppression was predicted at the relatively light mass targets than that found in heavy mass targets and a notably distinct dependence relationship was identified, suggesting that the predominant breakup mechanisms might change in different mass target regions. In addition, the minimum suppression factors are predicted to occur near the target nuclei with neutron closed shell.

Keywords: fusion reaction, weakly bound nuclei, machine learning, Bayesian neural network

I. INTRODUCTION

The advancements in beam quality and detection technology in the latest generation of radiation nuclear beam facilities have brought the study of reaction mechanisms induced by weakly bound nuclei at the Coulomb barrier energy region to the forefront of nuclear physics research [1–3]. In contrast to the fusion processes involving strongly bound nuclei, the mechanisms triggered by weakly bound nuclei are more complex due to their lower binding energies. This complexity is mainly exemplified by the extended nuclear matter distribution and the breakup effect [4, 5]. The former, a static effect, results in a reduction of the average fusion barrier height, consequently enhancing the fusion cross sections. While the dynamic breakup of the projectile can diminish the flux of direct fusion reactions and lead to three distinct processes: (1) sequential complete fusion (SCF), where all fragments resulting from the breakup fuse with the target; (2) incomplete fusion (ICF), where only part of the breakup fragments is absorbed by the target; and (3) no capture breakup (NCBU), where none of the breakup fragments are captured by target. The reaction process in which the whole projectile without breakup is captured by target is termed direct complete fusion (DCF). However, from the experimental perspective, it is challenging to differentiate between the fusion yields of SCF and DCF. As a result, only the complete fusion (CF) cross sections including both DCF and SCF cross sections can be measured.

Numerous experimental [6–9] and theoretical [10–12] studies have been performed on fusion reactions involving weakly bound nuclei over the last few decades. The main issue in these studies is to investigate the influence of the breakup on fusion reactions near the Coulomb barrier [13–15]. One of the most widely adopted approaches is to compare the date with the predictions from a single barrier penetration model (BMP) [16, 17] or a coupled channel model without the breakup channels [18–20]. It has been demonstrated that the CF cross sections are suppressed at energies near and above the Coulomb barrier [21, 22]. So far, the dependence of the suppression effect on the breakup threshold energy of the projectile has been revealed, and an empirical relationship between the suppression factors and the threshold energies is provided in ref. [23]. However, the suppression phenomena with various target nuclei remain incomprehensible [15, 24] and no systematic behavior of the CF suppression factors is observed at the relatively heavy mass target region [1]. For light and medium mass targets, the behavior of the suppression factor is not fully established due to the experimental difficulty in distinguishing residues from ICF and CF. Therefore, we have extended the machine learning method to the fusion reactions induced by weakly bound projectiles and analyzed the systematic behavior of suppression factors across various mass target regions.

Bayesian neural networks (BNNs), as one of the commonly used machine learning methods, have been applied to various issues in nuclear physics, such as predicting atomic nuclear mass [25, 26], nuclear charge radii [27, 28], nuclear β-decay half-life [29], nuclear fission yields [30–32], spallation reactions [33–35], and fragmentation reactions [36–38]. In this paper, based on the 475 experimental data points from 39 reaction systems all induced by ^{6,7}Li, ^{9}Be and ^{10}B, a Bayesian neural network was constructed to evaluate the CF cross sections of weakly bound nuclei. A systematic analysis of the suppression effect at energies above Coulomb barrier has also been conducted. The paper is organized as follows. In Sec. II, the main characteristics of the BNN method are briefly described. The prediction results are discussed in Sec. III. Sec. IV presents a summary.

* Supported by the National Natural Science Foundation of China (Grants No. 12105080 and No. 12375123), the China Postdoctoral Science Foundation (Grants No. 2023M731015), and the Natural Science Foundation of Henan Province (No. 242300422048).

† chengkaixuan@htu.edu.cn
‡ machunwang@126.com

II. MODEL DESCRIPTIONS

As a prominent machine learning technology, Bayesian neural networks are highly effective in constructing novel models based on the existing date. Comprising a specific number of input units, hidden units of several layers, and output units, BNNs are capable of delivering high-quality predictions. Here, a simple description of the BNN methodology is given. More detailed information can be found in refs. [33, 36] and cited therein.

The Bayesian learning sets the prior distribution $p(\omega)$ of the model through the network parameter ω before observing any data, and updates the prior distribution to the posterior distribution $p(\omega|D)$ by observing the experimental data $D(x_i^n, y_j^n)$,

$$p(\omega|D) = \frac{p(D|\omega)p(\omega)}{p(D)} \propto p(D|\omega)p(\omega), \tag{1}$$

where the prior distribution is a Gaussian distribution with zero mean and derived from the initial knowledge of the model. In the observed data $D(x_i^n, y_j^n)$, the outputs y_j^n corresponds to each inputs x_i^n where n,i,j are the number of date, inputs and outputs, respectively. The normalization function, $p(D)$, which ensures the posterior distribution in the effective probability density, is obtained through the model assumptions with a prior integral,

$$p(D) = \int p(D|\omega)p(\omega)d\omega. \tag{2}$$

The likelihood function $p(D|w)$ is based on the Gaussian distribution of the objective function χ^2, which fits the data by least squares,

$$p(D|\omega) = \exp(-\chi^2/2), \tag{3}$$

$$\chi^2 = \sum_{i=1}^{N} \left[\frac{y_j^n - f_k^n(x_i^n;\omega)}{\Delta y_j^n} \right]^2. \tag{4}$$

Here, Δy_j^n is the Gaussian noise corresponding to the nth observation. The feed-forward neural network is used for the BNN, which structure typically includes a set of input variables, several hidden layers, and one or more output variables. A typical network function that connects outputs y_j^n to inputs x_i^n through one hidden layer is shown as follows,

$$f_k^n(x_i^n;\omega) = a_k + \sum_{j=1}^{N} b_{jk} \tanh(c_j + \sum_{i=1}^{I} d_{ij} x_i^n), \tag{5}$$

where N and I are the numbers of hidden units and inputs. (d_{ij}, c_j) and (b_{jk}, a_k) are the weights and biases of the hidden and output layers, respectively. The hidden unit values are obtained by weighted summation of the input values acting on a hyperbolic tangent activation function (tanh), and the outputs $f_k^n(x_i^n;\omega)$ are obtained by weighted summation of the hidden unit values plus biases. The predicted distribution of output y_j^{n+1} corresponding to the new input x_i^{n+1} can be obtained from the posterior distribution,

$$p(y_j^{n+1}|x_i^{n+1}, D) = \int p(y_j^{n+1}|x_i^{n+1}, \omega)p(\omega|D)d\omega. \tag{6}$$

In the process of calculating output data of the model, Markov chain Monte Carlo method was used to solve the high-dimensional integral,

$$< y_j^{n+1} >= \frac{1}{K} \sum_{k=1}^{K} \int f_k^n(x_i^{n+1};\omega_k), \tag{7}$$

where K is the number of iteration samples. The uncertainty of predictions is obtained by $\Delta y_j = \sqrt{< y_j^2 > - < y_j >^2}$ because the model parameters are described with a probability distribution.

In this paper, the dataset comprises the measured CF cross sections in 39 reactions all induced by ^{6,7}Li, ^{9}Be and ^{10}B with 475 data points as detailed in Table 1. Within this dataset, the incident energy of the reactions ranges from $0.67V_b$ to $2.06V_b$, where V_b is the Coulomb barrier energies obtained from Akyüz-Winther nuclear potential and point-sphere Coulomb potential. The mass and charge of the target nuclei fall within the ranges of $64 \leq A_t \leq 209$ and $28 \leq Z_t \leq 83$, respectively. For model development, 80% of the data was randomly selected to form the training set, facilitating the neural networks learning and parameter optimization. The remaining 20% serves as the test set for evaluating the prediction capabilities of the network. The input layer contains five parameters: $\{Z_p, A_p, Z_t, A_t, E_{cm}\}$. Here, Z_p and A_p represent the proton and mass numbers of the projectiles, while Z_t and A_t correspond to those of the targets. The parameter E_{cm} denotes the center-of-mass energy in MeV. The output parameter is the CF cross section, σ_{exp}. Extensive efforts have been made to construct the hidden units, exploring both single-layer and double-layer configurations. The double-layer with 16 +16 neural units was ultimately verified as the most effective.

III. RESULTS AND DISCUSSIONS

In order to verify the evaluation capacity of BNN model, we perform a comparison between the predicted CF cross sections and the experimental data in Fig. 1. Taking the ^{6}Li + ^{159}Tb, ^{7}Li + ^{209}Bi, ^{9}Be + ^{89}Y, and ^{10}B + ^{159}Tb systems from the dataset as examples, the predicted results are in good agreement with the experimental CF cross sections, both at sub-barrier energies (Fig. 1(a)) and above barrier energies (Fig. 1(b)). Furthermore, for reaction system ^{8}Li + ^{208}Pb [67], which is not included in the dataset, the BNN model also gives the consistent results with the experiment data.

To further investigate the effects of the breakup channel on the fusion of weakly bound systems, a systematic analysis of the suppression factors of CF cross sections at above barrier energies is presented below. The suppression factors are calculated by comparing the CF cross sections obtained from the BNN model or the experimental data with those calculated by

Table 1. The 39 fusion systems induced by weakly bound projectile nuclei ^{6,7}Li, ^{9}Be and ^{10}B. The symbols E_{cm} and V_b are the center-of-mass energy and Coulomb barrier energy, respectively. N_{exp} gives the numbers of experimental CF cross section. F_{BNN} and F_{exp} denote the suppression factors calculated by Ep. (8). The last column is the corresponding reference where the measured cross sections are taken from.

Reaction	E_{cm}/V_B	N_{exp}	F_{BNN}	F_{exp}	Ref.	Reaction	E_{cm}/V_B	N_{exp}	F_{BNN}	F_{exp}	Ref.
^{6}Li+^{64}Ni	0.85-2.06	15	0.87	0.88	[39]	^{7}Li+^{159}Tb	1.07-1.66	5	0.71	0.73	[55]
^{6}Li+^{90}Zr	0.82-1.65	8	0.67	0.7	[18]	^{7}Li+^{165}Ho	0.86-1.69	10	0.79	0.74	[16]
^{6}Li+^{94}Zr	0.89-1.68	5	0.52	0.49	[8]	^{7}Li+^{197}Au	0.81-1.50	8	0.84	0.86	[48]
^{6}Li+^{96}Zr	0.90-1.58	7	0.77	0.77	[40]	^{7}Li+^{198}Pt	0.79-1.52	6	0.72	0.77	[56]
^{6}Li+^{120}Sn	0.74-1.32	13	0.78	0.81	[41, 42]	^{7}Li+^{205}Tl	0.82-1.31	10	0.77	0.74	[57]
^{6}Li+^{124}Sn	0.83-1.70	15	0.72	0.66	[43]	^{7}Li+^{209}Bi	0.83-1.67	21	0.75	0.77	[51]
^{6}Li+^{144}Sm	0.79-1.58	11	0.55	0.54	[44]	^{9}Be+^{89}Y	0.83-1.39	15	0.78	0.75	[58]
^{6}Li+^{152}Sm	0.80-1.60	20	0.63	0.62	[45]	^{9}Be+^{93}Nb	0.85-1.45	7	0.85	0.90	[59]
^{6}Li+^{154}Sm	1.04-1.45	6	0.64	0.71	[46]	^{9}Be+^{124}Sn	0.90-1.33	13	0.73	0.75	[60]
^{6}Li+^{159}Tb	0.87-1.50	13	0.65	0.66	[47]	^{9}Be+^{144}Sm	0.89-1.31	10	0.92	0.94	[61]
^{6}Li+^{197}Au	0.84-1.35	16	0.61	0.60	[48]	^{9}Be+^{169}Tm	0.93-1.33	12	0.78	0.80	[62]
^{6}Li+^{198}Pt	0.67-1.14	10	0.75	0.75	[49]	^{9}Be+^{181}Ta	0.94-1.34	13	0.66	0.68	[63]
^{6}Li+^{208}Pb	0.92-1.28	20	0.67	0.69	[50]	^{9}Be+^{186}W	1.08-1.40	4	0.59	0.57	[64]
^{6}Li+^{209}Bi	0.83-1.53	14	0.65	0.68	[51]	^{9}Be+^{187}Re	0.93-1.28	12	0.75	0.76	[62]
^{7}Li+^{64}Ni	0.87-2.06	16	0.90	0.90	[52]	^{9}Be+^{197}Au	0.83-1.17	12	0.78	0.70	[65]
^{7}Li+^{93}Nb	1.29-1.63	4	0.75	0.75	[53]	^{9}Be+^{208}Pb	0.88-1.24	16	0.78	0.79	[51]
^{7}Li+^{119}Sn	0.72-1.30	15	0.93	0.94	[41, 42]	^{9}Be+^{209}Bi	0.88-1.21	19	0.98	0.98	[50]
^{7}Li+^{124}Sn	0.79-1.86	23	0.71	0.73	[54]	^{10}B+^{159}Tb	0.91-1.66	16	0.87	0.87	[55]
^{7}Li+^{144}Sm	0.88-1.59	14	0.63	0.63	[19]	^{10}B+^{209}Bi	1.06-1.44	5	0.88	0.89	[66]
^{7}Li+^{152}Sm	0.81-1.61	16	0.66	0.69	[19]						

the single barrier potential model, as follows,

$$F_{BNN} = \frac{\sigma_{BNN}}{\sigma_{BPM}} \quad \text{or} \quad F_{exp} = \frac{\sigma_{exp}}{\sigma_{BPM}}, \tag{8}$$

where σ_{BNN} and σ_{exp} are the predicted and measured cross sections, respectively, and σ_{BPM} denotes the cross sections calculated by single barrier potential model. The calculated suppression factors using the predicted CF cross sections and experimental data are listed in the fourth and fifth columns of Table 1. To a large extent, the predictions of BNN model could represent the experimental suppression factors well. A detailed relationship between the suppression factor and the mass number of target nucleus A_t for ^{6}Li and ^{7}Li is shown in Fig. 2(a), and the corresponding results for ^{9}Be and ^{10}B shown in Fig. 2(b). Those target nuclei are mainly located in the relatively heavy mass region and no obvious dependence behavior can be found. In Fig. 2(a), it is evident that the suppression factor of ^{7}Li is larger than the one of ^{6}Li for the same mass target nuclei, which is attributed to the higher breakup threshold energies of ^{7}Li [23].

Next, we extend this BNN model to the various mass regions of the target nucleus, including the relatively light and medium mass targets. The CF cross sections of ^{6,7}Li and ^{9}Be with the target nuclei along β stability line are predicted. The calculated suppression factors versus the neutron, proton, and mass number of targets are shown in Fig. 3. A surprising conclusion is that there is no suppression effect in the vicinity of $A_t = 110$ targets for ^{6,7}Li and ^{9}Be, as well as $A_t = 180$ targets for ^{6,7}Li. This is derived from the overall trend of the available experimental data, and further experimental CF cross sections are necessary to verify this conclusion.

In Fig. 3, the solid symbols denote the mean suppression factors derived from the targets with identical neutron (a), proton (b), and mass (c) numbers . The dashed error bars illustrate the corresponding distribution range. Taking lead isotopes as an example, the predicted suppression factors of BNN model for ^{7}Li + ^{204,206,207,208}Pb are 0.78, 0.77, 0.76, and 0.75, respectively. The mean suppression factor (0.765), the upper limit of the error bar (0.78), and the lower limit of the error bar (0.75) are located at Z_t = 82 in the Fig. 3(b). Consequently, the range of error bars indicates the dependence relationship of the suppression effect on the isotones, isotopes, and isobars target nuclei. The small error bars of ^{6}Li and ^{7}Li suggest a weak dependence, whereas the suppression

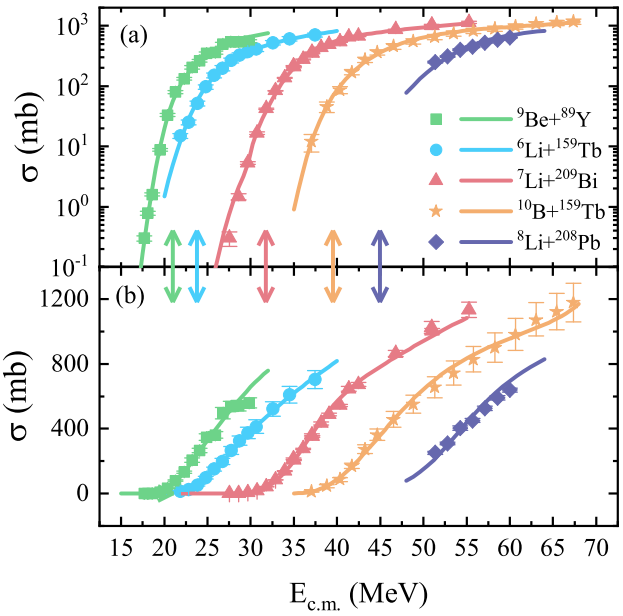

Fig. 1. Comparison of the CF cross sections obtained from the BNN model (solid lines) with the experimental data (solid symbols) for ^{6}Li + ^{159}Tb, ^{7}Li + ^{209}Bi, ^{9}Be + ^{89}Y, ^{10}Be + ^{159}Tb, and ^{8}Li + ^{208}Pb systems. The logarithmic scale and linear scale are shown in (a) and (b), respectively. The arrows give the corresponding Coulomb barrier energies. Note that the energies for ^{7}Li + ^{209}Bi and ^{8}Li + ^{208}Pb are shifted by 1.1 and 1.6, respectively.

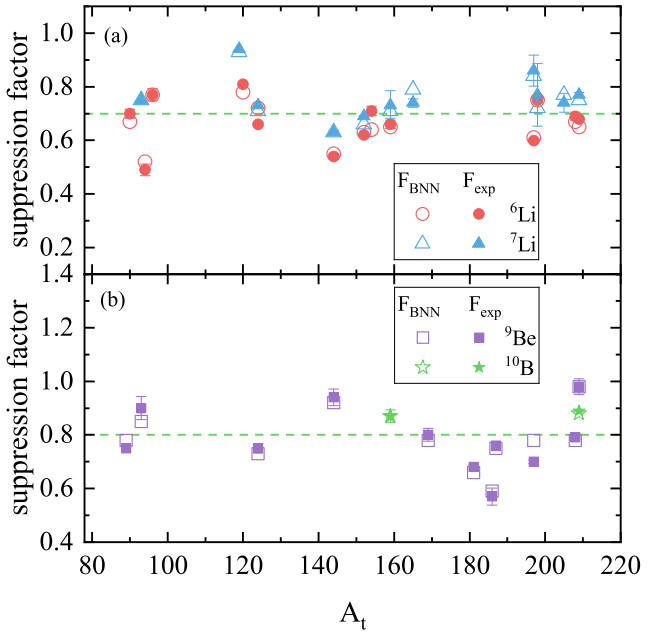

Fig. 2. The suppression factors obtained from the BNN model (open symbols) and experimental data (full symbols) for fusion systems listed in the Tab. 1. The reaction systems induced by ^{6}Li, ^{7}Li, ^{9}Be, and ^{10}B are represented by circles, triangles, squares, and stars, respectively. The horizontal dashed lines are the eye guidance reference lines.

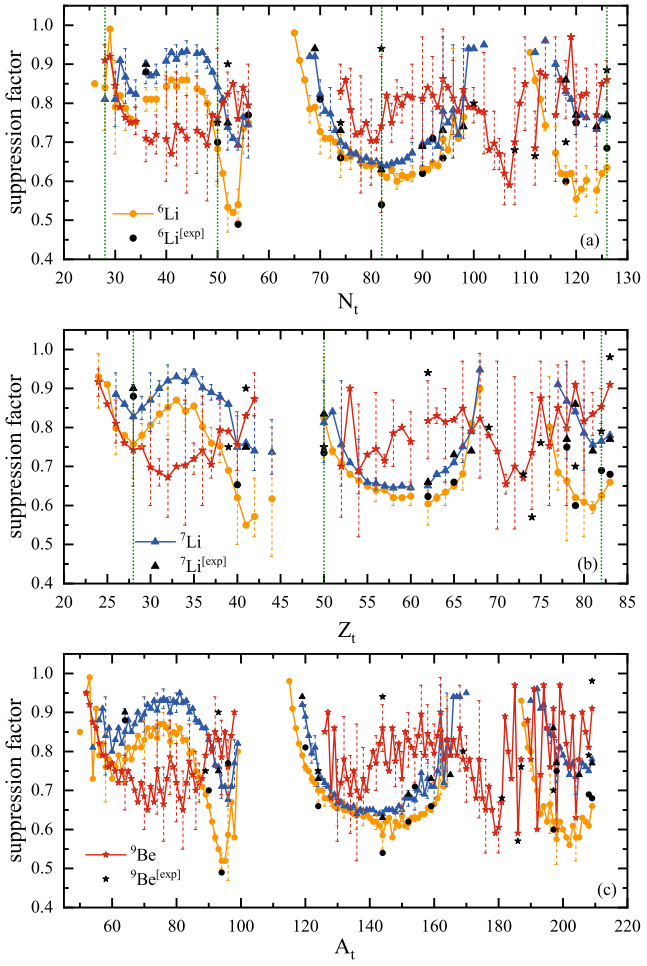

Fig. 3. The relationship between the suppression factors and the neutron (a), proton (b), and mass (c) number of the target nuclei for projectile nuclei ^{6}Li (circle), ^{7}Li (triangle), and ^{9}Be (star). The symbols denote the mean suppression factor and the dashed error bars indicate the distribution range. The magic numbers are located by the vertical dotted lines. The solid lines guide the eye. (See the text for more details.)

factors of ^{9}Be exhibit a strong dependence. Due to this sensitivity to the nucleon number of the target nucleus, there is a pronounced fluctuation at various target nuclei for ^{9}Be. This, to some extent, brings a difficulty in identifying the systematic trend for ^{9}Be.

In the cases of ^{6}Li and ^{7}Li, the consistent behavior of the mean suppression factor suggests that they possess the similar breakup mechanism, as well as the minimum values of the suppression factor both occurring near the target nuclei with neutron closed shell. Within the relatively light mass target region ($60 \leq A_t \leq 90$), the suppression factors for ^{6}Li and ^{7}Li remain around respectively 0.8 and 0.9, which is significantly less suppression compared to that observed for heavy targets ($120 \leq A_t \leq 160$). Moreover, the systematic behaviors in different mass target regions are markedly distinct. For light mass targets, the suppression factor varies with the target nucleus mass number, initially increasing and

then decreasing. In contract, at the heavy mass target region, the suppression factor initially decreases and then increases. This indicates that there is a competitive process in the breakup mechanism and the primary breakup channel may differ across various mass target regions. Due to the limitations of machine learning and complexity of the breakup processes, it is challenging to provide the specific physical mechanism here. More experimental and theoretical research is needed to verify these conclusions and provide more explanations for the underlying breakup mechanism.

IV. SUMMARY

In this paper, we investigate the complete fusion reactions of weakly bound nuclei using machine learning methods. Based on the 475 existing experimental complete fusion data induced by ^{6,7}Li, ^{9}Be and ^{10}B, a Bayesian neural network is construct. This model characterizes 5 input parameters (projectile and target information, colliding energy) , double hidden layers (16+16 neural units), and one output parameter (CF cross section). The CF cross sections predicted by this model exhibit an excellent agreement with the experimental data, demonstrating the model's high-quality predictive capagilities.

The suppression factors, defined as the ratio of the predicted CF cross sections by BNN model to those calculated by the single barrier penetration model at above barrier energies, have been systematically analyzed for weakly bound projectiles ^{6,7}Li and ^{9}Be with the target nuclei along the β stability line. The dependence behavior of the suppression effect has been predicted across various mass target regions, especially for the relatively light mass targets. For ^{9}Be, the suppression factors exhibit marked sensitivity to the target nucleus and no apparent systematic behavior could be observed in either the heavy or light mass target regions. In contrast, for ^{6}Li and ^{7}Li, the BNN model predictd a less suppression in relatively light mass targets compared to that observed for heavy mass targets. Furthermore, the dependence at the light mass target region is exactly opposite to that at the heavy mass target region. These conclusions require further experimental and theoretical validation, as well as the mechanism explanations.

[1] L. F. Canto, P. R. S. Gomes, R. Donangelo et al., Recent developments in fusion and direct reactions with weakly bound nuclei. Phys. Rept. **596**, 1 (2015). http://dor.org/10.1016/j.physrep.2015.08.001

[2] Y. L. Ye, X. F. Yang, H. Sakurai et al., Physics of exotic nuclei. Nat. Rev. Phys. **7**, 21-37 (2024). https://doi.org/10.1038/s42254-024-00782-5

[3] T. P. Luo, L. Yang, C. J. Lin et al., Reaction dynamics of proton-rich nuclei at energies around the Coulomb barrier: the cases of ^{7}Be, ^{8}B, and ^{17}F. Nucl. Sci. Tech. **35**, 212 (2024). https://doi.org/10.1007/s41365-024-01586-z

[4] L. F. Canto, V. Guimaraes, J. Lubian et al., The total reaction cross section of heavy-ion reactions induced by stable and unstable exotic beams: the low-energy regime. Eur. Phys. J. A **56**, 281 (2020). https://doi.org/10.1140/epja/s10050-020-00277-8

[5] K. Hagino, K. Ogata, and A. Moro, Coupled-channels calculations for nuclear reactions: From exotic nuclei to superheavy elements. Prog. Part. Nucl. Phys. **125**, 103951 (2022). https://doi.org/10.1016/j.ppnp.2022.103951

[6] L. Yang, C. J. Lin, H. Yamaguchi et al., Breakup of the proton halo nucleus ^{8}B near barrier energies. Nat. Commun. **13**, 7193 (2022). https://doi.org/10.1038/s41467-022-34767-8

[7] G. L. Zhang, Z. W. Jiao, G. X. Zhang et al., Further investigation on the fusion of ^{6}Li with ^{209}Bi target at near-barrier energies. Chin. Phys. C **48**, 074001 (2024). https://doi.org/10.1088/1674-1137/ad4264

[8] X. D. Su, G. X. Zhang, S. P Hu et al., Fusion and one-neutron stripping process for ^{6}Li + ^{94}Zr system around the Coulomb Barrier. Chin. Phys. C **48**, 094001 (2024). https://doi.org/10.1088/1674-1137/ad50b9

[9] Y. D. Fang, P. R. S. Gomes, J. Lubian et al., Complete and imcomplete fusion of ^{9}Be + ^{169}Tm, ^{187}Re at near barrier energies. Phys. Rev. C **91**, 014608 (2015). https://doi.org/10.1103/PhysRevC.91.014608

[10] A. D. Torres, D. J. Hinde, J. A. Tostevin et al., Relating Breakup and Incomplete Fusion of Weakly Bound Nuclei through a Classical Trajectory Model with Stochastic Breakup. Phys. Rev. Lett. **98**, 152701 (2007). https://doi.org/10.1103/PhysRevLett.98.152701

[11] L. Jin and A. M. Moro, Puzzle of complete fusion suppression in weakly bound nuclei: a trojan horse effect? Phys. Rev. Lett. **122**, 042503 (2019). https://doi.org/10.1103/PhysRevLett.122.042503

[12] L. Jin and A. M. Moro, Unraveling the reaction mechanisms leading to partial fusion of weakly bound nuclei. Phys. Rev. Lett. **123**, 232501 (2019). https://doi.org/10.1103/PhysRevLett.123.232501

[13] M. Dasgupta, L. R. Gasques, D. H. Luong et al., Reaction dynamics of weakly bound nuclei at near-barrier energies. Nucl. Phys. A **834**, 147c–150c (2010). http://dx.doi.org/10.1016/j.nuclphysa.2009.12.025

[14] P. R. S. Gomes, D. R. Otomar, T. Correa et al., Complete fusion enhancement and suppression of weakly bound nuclei at near barrier energies. J. Phys. G: Nucl. Part. Phys. **39**, 115103 (2012). http://dx.doi.org/10.1088/0954-3899/39/11/115103

[15] V. V. Sargsyan, G. G. Adamian, N. V. Antonenko et al., Search for a systematic behavior of the breakup probability in reactions with weakly bound projectiles at energies around the Coulomb barrier. Phys. Rev. C **86**, 054610 (2012). http://dx.doi.org/10.1103/PhysRevC.86.054610

[16] V. Tripathi, A. Navin, K. Mahata et al., Angular Momentum and Cross Sections for Fusion with Weakly Bound Nuclei: Breakup, a Coherent Effect. Phys. Rev. Lett. **88**, 172701 (2002). http://dx.doi.org/10.1103/PhysRevLett.88.172701

[17] V. Tripathi, A. Navin, V. Nanal et al., Experimental signatures for distinguishing breakup fusion and transfer in ^{7}Li $+^{165}$ Ho. Phys. Rev. C **72**, 017601 (2005). http://dx.doi.org/10.1103/PhysRevC.72.017601

[18] H. Kumawat1, V. Jha1, V. V. Parkar et al., Fusion reaction studies for the ^{6}Li + ^{90}Zr system at near-

barrier energies. Phys. Rev. C **86**, 024607 (2012). http://dx.doi.org/10.1103/PhysRevC.86.024607

[19] P. K. Rath1, S. Santra, N. L. Singh et al., Complete fusion in ^{7}Li + ^{144,152}Sm reactions. Phys. Rev. C **88** 044617 (2013). http://dx.doi.org/10.1103/PhysRevC.88.044617

[20] K. X. Cheng, J. Pu, Y. T. Wang et al., Non-frozen process of heavy-ion fusion reactions at deep sub-barrier energies. Nucl. Sci. Tech. **33**, 132 (2022). https://doi.org/10.1007/s41365-022-01114-x

[21] S. P. Hu, G. L. Zhang, J. C. Yang et al., Small suppression of the complete fusion of the ^{6}Li + ^{96}Zr system at near-barrier energies. Phys. Rev. C **91**, 044619 (2015). https://doi.org/10.1103/PhysRevC.91.044619

[22] K. J. Cook, E. C. Simpson, L. T. Bezzina et al., Origins of imcomplete fusion products and the suppression of complete fusion in reactions of ^{7}Li, Phys. Rev. Lett. **122**, 102501 (2019). https://doi.org/10.1103/PhysRevLett.122.102501

[23] B. Wang, W. J. Zhao, P. R. S. Gomes et al., Systematic study of breakup effects on complete fusion at energies above the Coulomb barrier. Phys. Rev. C **90**, 034612 (2014). http://dx.doi.org/10.1103/PhysRevC.90.034612

[24] P. R. S. Gomes, R. Linares, J. Lubian et al., Search for systematic behavior of incomplete-fusion probability and complete-fusion suppression induced by ^{9}Be on different targets. Phys. Rev. C **84**, 014615 (2011). http://dx.doi.org/10.1103/PhysRevC.84.014615

[25] Z. M. Niu and H. Z. Liang, Nuclear mass predictions based on Bayesian neural network approach with pairing and shell effects. Phys. Lett. B **778**, 48 (2018). http://dx.doi.org/10.1016/j.physletb.2018.01.002

[26] Z. M. Niu and H. Z. Liang, Nuclear mass predictions with machine learning reaching the accuracy required by r-process studies. Phys. Rev. C **106**, L021303 (2022). http://dx.doi.org/10.1103/PhysRevC.106.L021303

[27] Y. F. Ma, C. Su, J. Liu et al., Predictions of nuclear charge radii and physical interpretations based on the naive Bayesian probability classifier. Phys. Rev. C **101**, 014304 (2020). http://dx.doi.org/10.1103/PhysRevC.101.014304

[28] X. X. Dong, R. An, J. X. Lu et al, Nuclear charge radii in Bayesian neural networks revisited. Phys. Lett. B **838**, 137726 (2023). https://doi.org/10.1016/j.physletb.2023.137726

[29] Z. M. Niu, H. Z. Liang, B. H. Sun et al., Predictions of nuclear β -decay half-lives with machine learning and their impact on r -process nucleosynthesis. Phys. Rev. C **99**, 064307 (2019). http://dx.doi.org/10.1103/PhysRevC.99.064307

[30] C. Y. Qiao, J. C. Pei, Z. A. Wang et al., Bayesian evaluation of charge yields of fission fragments of ^{239}U. Phys. Rev. C **103**, 034621 (2021). http://dx.doi.org/10.1103/PhysRevC.103.034621

[31] Z. A. Wang, J. C. Pei, Y. Liu et al., Bayesian Evaluation of Incomplete Fission Yields. Phys. Rev. Lett. **123**, 122501 (2019). http://dx.doi.org/10.1103/PhysRevLett.123.122501

[32] Z. A. Wang and J. C. Pei, Optimizing multilayer Bayesian neural networks for evaluation of fission yields. Phys. Rev. C **104**, 064608 (2021). http://dx.doi.org/10.1103/PhysRevC.104.064608

[33] C. W. Ma, D. Peng, H. L. Wei., Isotopic cross-sections in proton induced spallation reactions based on the Bayesian neural network method. Chin. Phys. C **44**, 014104 (2020). http://dx.doi.org/10.1088/1674-1137/44/1/014104

[34] C. W. Ma, D. Peng, H. L. Wei et al., A Bayesian-Neural-Network Prediction for Fragment Production in Proton Induced Spallation Reaction. Chin. Phys. C **44**, 124107 (2020). http://dx.doi.org/10.1088/1674-1137/abb657

[35] D. Peng, H. L. Wei, X. X. Chen et al., Bayesian evaluation of residual production cross sections in proton-induced nuclear spallation reactions. J. Phys. G: Nucl. Part. Phys. **49**, 085102 (2022). http://dx.doi.org/10.1088/1361-6471/ac7069

[36] C. W. Ma, X. B. Wei, X. X. Chen et al., Precise machine learning models for fragment production in projectile fragmentation reactions using Bayesian neural networks. Chin. Phys. C **46**, 074104 (2022). http://dx.doi.org/10.1088/1674-1137/ac5efb

[37] C. W. Ma, X. X. Chen, X. B. Wei et al., Systematic behavior of fragments in Bayesian neural network models for projectile fragmentation reactions. Phys. Rev. C **108**, 044606 (2023). http://dx.doi.org/10.1103/PhysRevC.108.044606

[38] X. B. Wei, H. L .Wei, Y. T. Wang et al., Multiple-models predictions for drip line nuclides in projectile fragmentation of ^{40,48}Ca, ^{58,64}Ni, and ^{78,86}Kr at 140MeV/u. Nucl. Sci. Tech. **33**, 155 (2023). https://doi.org/10.1007/s41365-022-01137-4

[39] M. M. Shaikh, S. Roy, S. Rajbanshi et al., Investigation of ^{6}Li + ^{64}Ni fusion at near-barrier energies. Phys. Rev. C **90**, 024615 (2014). http://dx.doi.org/10.1103/PhysRevC.90.024615

[40] S. P. Hu, G. L. Zhang, J. C. Yang et al., Small suppression of the complete fusion of the ^{6}Li + ^{96}Zr system at near-barrier energies. Phys. Rev. C **91**, 044619 (2015). http://dx.doi.org/10.1103/PhysRevC.91.044619

[41] N. Grover, I. Sharma, M. S. Gautam et al., Fusion and decay dynamics of ^{6}Li + ^{120}Sn and ^{7}Li + ^{119}Sn reactions across the Coulomb barrier. Phys. Rev. C **108**, 064607 (2023). http://dx.doi.org/10.1103/PhysRevC.108.064607

[42] M. Fisichella1, A. C. Shotter, P. Figuera1 et al., Breakup and n -transfer effects on the fusion reactions ^{6,7}Li + ^{120,119}Sn around the Coulomb barrier. Phys. Rev. C **95**, 034617 (2017). http://dx.doi.org/10.1103/PhysRevC.95.034617

[43] V. V. Parkar1, S. K. Pandit1, A. Shrivastava et al., Fusion reaction studies for the ^{6}Li + ^{124}Sn system at near-barrier energies. Phys. Rev. C **98**, 014601 (2018). http://dx.doi.org/10.1103/PhysRevC.98.014601

[44] P. K. Rath, S. Santra, N. L. Singh et al., Suppression of complete fusion in the ^{6}Li + ^{144}Sm reaction. Phys. Rev. C **79**, 051601 (2009). http://dx.doi.org/10.1103/PhysRevC.79.051601

[45] P. K. Rath, S. Santra, N. L. Singh et al., Fusion of ^{6}Li with ^{152}Sm: Role of projectile breakup versus target deformation. Nucl. Phys. A **874**, 14 (2012). http://dx.doi.org/10.1016/j.nuclphysa.2011.10.004

[46] C. L. Guo, G. L. Zhang, S. P. Hu et al., Coupling effects on the fusion of ^{6}Li + ^{154}Sm at energies slightly above the Coulomb barrier. Phys. Rev. C **92**, 014615 (2015). http://dx.doi.org/10.1103/PhysRevC.92.014615

[47] M. K. Pradhan, A. Mukherjee, P. Basu et al., Fusion of ^{6}Li with ^{159}Tb at near barrier energies. Phys. Rev. C **83**, 064606 (2011). http://dx.doi.org/10.1103/PhysRevC.83.064606

[48] C. S. Palshetkar1, S. Thakur, V. Nanal et al., Fusion and quasielastic scattering in the ^{6,7}Li + ^{197}Au systems. Phys. Rev. C **89**, 024607 (2014). [Erratum: Phys.Rev.C **100**, 039902 (2019)] http://dx.doi.org/10.1103/PhysRevC.89.024607

[49] A. Shrivastava, A. Navin, A. Lemasson et al., Exploring Fusion at Extreme Sub-Barrier Energies with Weakly Bound Nuclei. Phys. Rev. Lett. **103**, 232702 (2009). https://doi.org/10.1103/PhysRevLett.103.232702

[50] Z. H. Liu, C. Signorini, M. Mazzocco et al., Partial fusion of a weakly bound projectile with heavy target at energies above the Coulomb barrier. Eur. Phys. J. A **26**, 73 (2005). http://dx.doi.org/10.1140/epja/i2004-10305-4

[51] M. Dasgupta1, P. R. S. Gomes, D. J. Hinde et al., Effect of breakup on the fusion of ^{6}Li, ^{7}Li, and ^{9}Be with heavy nuclei. Phys. Rev. C **70**, 024606 (2004). http://dx.doi.org/10.1103/PhysRevC.70.024606

[52] M. M. Shaikh, S. Roy, S. Rajbanshi et al., Probing the fusion of ^{7}Li with ^{64}Ni at near-barrier energies. Phys. Rev. C **93**, 044616 (2016). http://dx.doi.org/10.1103/PhysRevC.93.044616

[53] S. K. Pandit1, A. Shrivastava, K. Mahata et al., Investigation of large α production in reactions involving weakly bound ^{7}Li. Phys. Rev. C **96**, 044616 (2017). http://dx.doi.org/10.1103/PhysRevC.96.044616

[54] V. V. Parkar, S. K. Sharma, R. Palit et al., Investigation of complete and incomplete fusion in the ^{7}Li + ^{124}Sn reaction near Coulomb barrier energies. Phys. Rev. C **97**, 014607 (2018). http://dx.doi.org/10.1103/PhysRevC.97.014607

[55] A. Mukherjee, S Roy, M. K. Pradhan et al., Influence of projectile alpha- breakup threshold on complete fusion. Phys. Lett. B **636**, 91 (2006) http://dx.doi.org/10.1016/j.physletb.2006.03.051

[56] A. Shrivastava, A. Navin, A. D. Torres et al., Role of the cluster structure of ^{7}Li in the dynamics of fragment capture. Phys. Lett. B **718**, 931 (2013). http://dx.doi.org/10.1016/j.physletb.2012.11.064

[57] V. V. Parkar, M. Prasanna, R. Ruchi et al., Fusion of ^{7}Li with ^{205}Tl at near-barrier energies. Phys. Rev. C **109**, 014610 (2024). http://dx.doi.org/10.1103/PhysRevC.109.014610

[58] C. S. Palshetkar, S. Santra, A. Chatterjee et al., Fusion of the weakly bound projectile ^{9}Be with ^{89}Y. Phys. Rev. C **82**, 044608 (2010). http://dx.doi.org/10.1103/PhysRevC.82.044608

[59] H. Sharma, M. Maiti, M. Sagwa etal ., Study of ^{9}Be fusion in ^{93}Nb near the Coulomb barrier. Eur. Phys. J. A **60**, 64 (2024). http://dx.doi.org/10.1140/epja/s10050-024-01296-5

[60] V. V. Parkar, R. Palit1, S. K. Sharma et al., Fusion cross sections for the ^{9}Be + ^{124}Sn reaction at energies near the Coulomb barrier. Phys. Rev. C **82**, 054601 (2010) http://dx.doi.org/10.1103/PhysRevC.82.054601

[61] P. R. S. Gomesa, J. Lubiana, B. Paes et al., Near-barrier fusion, breakup and scattering for the ^{9}Be + ^{144}Sm system. Nucl. Phys. A **828**, 233 (2009). http://dx.doi.org/10.1016/j.nuclphysa.2009.07.008

[62] Y. D. Fang, P. R. S. Gomes, J. Lubian et al., Complete and incomplete fusion of ^{9}Be + ^{169}Tm,^{187}Re at near-barrier energies. Phys. Rev. C **91**, 014608 (2015). http://dx.doi.org/10.1103/PhysRevC.91.014608

[63] N. T. Zhang, Y. D. Fang, P. R. S. Gomes et al., Complete and incomplete fusion in the ^{9}Be + ^{181}Ta reaction. Phys. Rev. C **90**, 024621 (2014). http://dx.doi.org/10.1103/PhysRevC.90.024621

[64] Y. D. Fang, P. R. S. Gomes, J. Lubian et al., Fusion and one-neutron stripping reactions in the ^{9}Be $+^{186}$W system above the Coulomb barrier. Phys. Rev. C **87**, 024604 (2013). http://dx.doi.org/10.1103/PhysRevC.87.024604

[65] M. Kaushik, G. Gupta, S. Thakur et al., Fusion of the Borromean nucleus ^{9}Be with a ^{197}Au target at near-barrier energies. Phys. Rev. C **101**, 034611 (2020). http://dx.doi.org/10.1103/PhysRevC.101.034611

[66] L. R. Gasques, D. J. Hinde, M. Dasgupta et al., Suppression of complete fusion due to breakup in the reactions ^{10,11}B + ^{209}Bi. Phys. Rev. C **79**, 034605 (2009). http://dx.doi.org/10.1103/PhysRevC.79.034605

[67] E. F. Aguilera, E. M. Quiroz, P. Rosales et al., Hindrance of complete fusion in the ^{8}Li + ^{208}Pb system at above-barrier energies. Phys. Rev. C **80**, 044605 (2009). http://dx.doi.org/10.1103/PhysRevC.80.044605